Carbon Nanomaterials

DOI: 10.1002/anie.201402574

Facile One-Pot, One-Step Synthesis of a Carbon Nanoarchitecture for an Advanced Multifunctonal Electrocatalyst**

*Zhenhai Wen, Suqin Ci, Yang Hou, and Junhong Chen**

Abstract: *A one-pot/one-step synthesis strategy was developed for the preparation of a nitrogen-doped carbon nanoarchitecture with graphene-nanosheet growth on the inner surface of carbon nanotubes (CNTs). The N-graphene/CNT hybrids exhibit outstanding electrocatalytic activity for several important electrochemical reactions as a result of their unique morphology and defect structures, such as high but uniform nitrogen doping, graphene insertion into CNTs, considerable surface area, and the presence of iron nanoparticles. The high-yield synthetic process features high efficiency, low-cost, straightforward operation, and simple equipment.*

There is no doubt that carbon nanotubes (CNTs) and graphene are representative 1D and 2D nanomaterials that have inspired tremendous research into nanomaterials in general and their application.[1] Graphene/CNT hybrids have recently drawn extensive attention because an integrated graphene/CNT hybrid offers the full advantages of the unique properties of both nanocarbons, including good flexibility, excellent electrical conductivity, and an impressive stretching ability.[2] Typically, graphene/CNT hybrids can be prepared through multistep processes that include:[2d,3] 1) the separate synthesis of graphene and CNTs, and 2) the assembly of CNTs and graphene. Although these methods may successfully produce well-organized graphene/CNT hybrids, they inevitably require various additional pre- or postsynthetic processes, such as chemical modification, centrifuging, catalyst preparation, and multiple fabrication/synthesis steps.

Owing to their unique nanostructure and attractive properties, graphene/CNT hybrids are promising for applications in fuel cells, biosensors, optoelectronic devices, lithium-ion batteries, supercapacitors, and nanoelectronics.[4] For example, the Tour research group demonstrated, by using plasma-assisted chemical vapor deposition (CVD), that the combination of graphene with CNTs into a seamless 3D structure with forests of carbon nanotubes grown on graphene was of great potential for the fabrication of high-performance supercapacitor devices.[5] However, most of the graphene/CNT hybrids reported to date feature CNT growth or assembly on the surface of graphene.

The Dai research group reported an appealing electrocatalyst for the oxygen-reduction reaction (ORR) on the basis of nitrogen-doped graphene/CNT complexes, in which nanoscale graphene sheets were attached to the external surface of CNTs by partly exfoliating the outer wall of multiwalled carbon nanotubes.[6] Lv et al. reported an interesting N-graphene/CNT hybrid in which small graphene layers were distributed inside the inner cavities of CNTs by a water-assisted CVD route.[7] However, the synthetic route, just like the conventional CVD method, is limited to the use of gaseous small molecules and suffers from the major disadvantages of a long reaction time and a low yield. Moreover, H_2 gas and water vapor were necessary to assist the growth of such hybrids. Recently, synthesis from solid-phase precursors was reported as a promising complementary method for the production of carbon nanoarchitectures.[8] In parallel to their synthesis, the exploration of the functionality and potential applications of N-graphene/CNT hybrids has become an area of further growth.

We herein demonstrate the use of a one-pot, one-step strategy to prepare a nitrogen-doped carbon nanoarchitecture in which graphene nanosheets are entrapped on the inner surface of CNTs (N-graphene/CNT hybrids). The synthesis was accomplished through a simple and convenient experimental setup (Figure 1 a) by annealing a powder mixture of $FeCl_3$ and cyanamide at 900 °C under an Ar atmosphere, during which the Fe^{3+} ions were reduced to Fe nanocatalysts to assist the evolution of gases released from the decomposition of cyanamide into N-graphene/CNT hybrids (Figure 1 b). This evolution process was directly reflected by the change in the sample color from brown to black (Figure 1 c).

Figure 1 d,e shows typical low-magnification scanning electron microscopy (SEM) images of the N-graphene/CNT hybrids, from which one can see large filament bundles that look like grass arrays. Black dots observed at the tip of the tube in an SEM image of a N-graphene/CNT (Figure 1 f) were shown to be nanoparticles on the basis of additional SEM and TEM images (see Figure S1 in the Supporting Information). Figure 1 g–i displays transmission electron microscopy (TEM) images of N-graphene/CNTs at different magnifications. A large number of "stripes" are apparent on the nanotubes, and some nanoparticles are sparsely dispersed in the tube. These "stripes" are actually graphene nanosheets entrapped in the inner void of CNTs. The "stripes" are slightly obscure as compared with the wall of CNTs, thus indicating that the stripes are actually inside the CNT (see Figure S2). Furthermore, these "stripes" have a well-defined graphite structure

[*] Dr. Z. Wen,[+] Dr. S. Ci,[+] Dr. Y. Hou, Prof. J. Chen
Department of Mechanical Engineering
University of Wisconsin-Milwaukee
3200 North Cramer Street, Milwaukee, WI 53211 (USA)
E-mail: jhchen@uwm.edu

[+] These authors contributed equally.

[**] This research was financially supported by the National Natural Science Foundation of China (No. 21206068), the US National Science Foundation (CMMI-0900509), and the US Department of Energy (DE-EE0003208).

Supporting information for this article is available on the WWW under http://dx.doi.org/10.1002/anie.201402574.

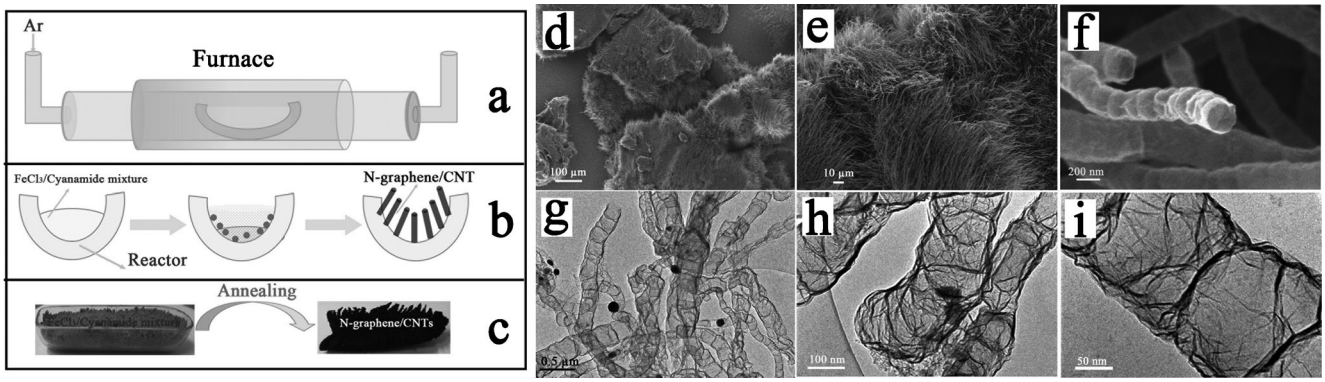

Figure 1. a) Experimental setup and b) schematic mechanism for the synthesis of N-graphene/CNT hybrids. c) Photographic images of samples before (brown) and after annealing (black). d–f) SEM and g–i) TEM images of the N-graphene/CNT hybrids at different magnifications.

with an interlayer *d*-spacing of around 0.34 nm (see Figure S2 c,d).

We conducted controlled synthetic experiments to study the effect of the cyanamide/$FeCl_3$ molar ratio on the structure and morphology of the products. At a high cyanamide/$FeCl_3$ molar ratio of 300, CNTs grew in sections connected with a "knot" to construct a well-defined bamboolike structure with a diameter ranging from 20 to 60 nm (see Figure S3 a,b). Such bamboolike CNTs, then formed by a CVD method, have been reported previously.[9] The N-graphene/CNT hybrid was found to be produced with a cyanamide/$FeCl_3$ molar ratio of about 100. The diameter of the N-graphene/CNT was estimated to be in the range of 100–200 nm, and is thus much larger than that of bamboolike CNTs. Therefore, the graphene nanosheets in the inner void of CNTs must be derived from the "knots" of bamboolike CNTs. The reason that they do not form closed "knots" is because the CNT diameter is so large (over 100 nm) that the graphite nanosheets can only grow into small nanosheets rather than form "knots". When the ratio of cyanamide/$FeCl_3$ was decreased to 30 (see Figure S3 c,d) and 10 (Figure S3 e,f), the products tended to be core–shell structures with iron-based composite nanorods as the core and a carbon film as the shell.[10]

On the basis of the results of the controlled experiments and TEM analysis, we propose a plausible mechanism to illustrate the growth of N-graphene/CNT hybrids. In this study, cyanamide was chosen as the source of carbon and nitrogen, and $FeCl_3$ as the catalyst precursor. Because the cyanamide and $FeCl_3$ are mixed thoroughly, Fe^{3+} should be uniformly dispersed or adsorbed on the cyanamide powder at the initial stage of the heating process. Subsequent annealing led to the polyaddition and polycondensation of cyanamide with the formation of polymeric carbon nitrides. Meanwhile, Fe^{3+} was reduced to Fe nanocatalysts by either polymeric carbon nitrides or reducing gases released during the polymerization of cyanamide. There were no CNTs among the products obtained at 550 °C (see Figure S4 a,b). Upon heating to a temperature above 700 °C, the N-graphene/CNT hybrid was obtained, as reflected by the samples obtained at 750 °C (see Figure S4 c,d). Above 700 °C, the polymeric carbon nitrides are thought to decompose and generate a large number of cyano fragments (e.g., $C_2N_2^+$, $C_3N_2^+$, $C_3N_3^+$),[11] which serve as carbon sources for CNT growth and nitrogen sources for nitrogen-doping reactions. As a result, CNTs precipitate out across the Fe nanoparticles, thus driving continued growth of CNTs and pushing the entire metal particle off the substrate by a well-known "tip-growth mode".[12] At a low fraction of the Fe source, the resulting Fe nanoparticles are small, thus leading to the formation of CNTs with a relatively small diameter. With an increasing ratio of Fe^{3+}, the CNTs grow larger as Fe catalyst nanoparticles become larger. The graphene sheets are formed inside the CNTs as a result of the defects due to nitrogen doping, the relatively low growth rate of graphite nanosheets, and the large voids of as-formed CNTs.[9c] With a further increase in the Fe fraction, iron-based core–shell structures are produced through the oriented attachment of Fe nanoparticles and the subsequent growth of a graphite shell.[10]

The present strategy for the synthesis of this unique carbon nanoarchitecture has several advantages. First of all, the synthetic procedure is quite simple: it can be implemented as a one-pot, one-step process by the annealing of solid sources. Second, this method is highly effective and efficient with potential for high-yielding production; it takes less than 10 h to complete the entire process with a yield as high as about 15% as based on the total mass of reactants. Furthermore, nitrogen can be uniformly doped in the carbon nanoarchitecture as a result of the high nitrogen content in cyanamide. Uniform nitrogen doping significantly enhances the functional properties of the material for catalysis and biocompatibility.[9a,13] Furthermore, the hybrids have an open-end structure with graphene nanosheets decorating the CNT voids. This unique structure may unify the merits of CNTs and graphene. Last but not least, there is no special or expensive equipment needed except for an annealing device and a protecting gas (Ar) environment. Thus, the process could potentially meet the requirements for large-scale production owing to its low cost, straightforward operation, simple equipment, and high yield.

We further studied the composition, crystalline structure, surface properties, and porous structure of the N-graphene/CNT hybrids by using various techniques, such as energy-dispersive X-ray spectroscopy (EDS), X-ray diffraction (XRD), N_2 adsorption–desorption, X-ray photoelectron spectroscopy (XPS), and Raman spectroscopy. According to EDS, the N-graphene/CNT hybrids contain around 3.5 atom% Fe, 89.9 atom% C, and 6.6 atom% N (see Figure S5). Figure 2 a shows the XRD pattern of the N-graphene/

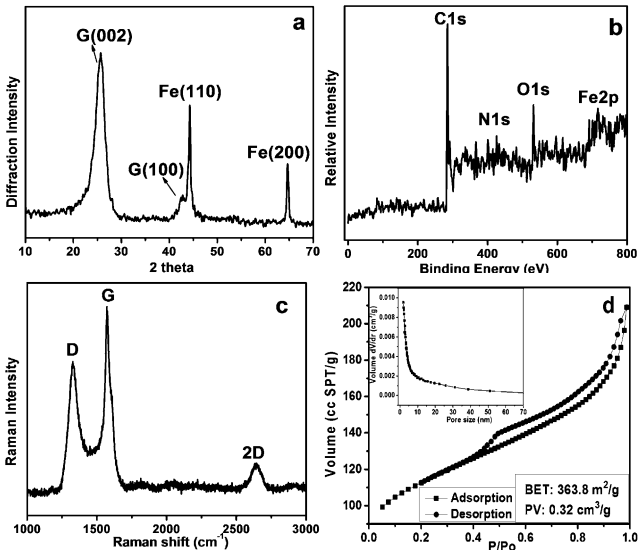

Figure 2. a) XRD pattern, b) XPS spectrum, c) Raman spectrum, and d) nitrogen adsorption–desorption isotherm and BJH pore-size distribution derived from the adsorption branch of the isotherm (inset) of the N-graphene/CNT hybrids. STP = standard temperature and pressure.

CNT hybrids. Two characteristic diffraction peaks at 26.1 and 43.2° are attributed to the graphite (002) and (100) planes, and the other two peaks at 44.3 and 64.6° coincide well with the (110) and (200) planes, respectively, of γ-Fe, thus demonstrating that the composites consist of Fe and graphitic carbon. Figure 2b displays the survey XPS spectrum of the N-graphene/CNT hybrids, in which a set of peaks correspond to C 1s (285.1), O 1s (531.6 eV), N 1s (399.1 eV), and Fe 2p (712.9 eV) spectra. The high-resolution XPS spectra (see Figure S6) reveal that the N 1s peak can be fitted to four different types of N atom: pyridine-type N (398.2 eV), pyrrole-type N (399.9 eV), graphite-type N (401.2 eV), and pyridine *N*-oxide (402.1 eV).[14] The D and G bands in the Raman spectrum are positioned at 1329 and 1573 cm^{-1}, respectively (Figure 2c). The intensity ratio of the D to the G band is about 0.7, and the I_G/I_{2D} ratio is around 6, which is characteristic of graphite with a defective structure.[8a,15] The nitrogen-adsorption–desorption-isotherm curve of the N-graphene/CNT hybrids (Figure 2d) shows a hysteresis loop at a relative pressure P/P_0 of 0.4–1, which corresponds to the type IV isotherm. The N-graphene/CNT hybrid has a BET surface area of 363.8 $m^2 g^{-1}$ and a pore volume of 0.32 $cm^3 g^{-1}$. Analysis of the pore-size distribution by using the BJH (Barrett–Joyner–Halenda) method applied to the adsorption branch of the isotherm (inset in Figure 2d) indicated that the pores in the meterial were mesopores with a broad pore-size distribution.

We carried out electrochemical tests with a glass carbon electrode (GCE) modified with the N-graphene/CNT hybrid to investigate the electrocatalytic activity of the material for a series of important electrochemical reactions: ORR, water oxidation, and redox reactions of the three molecular probes hydrogen peroxide, dopamine (DA), and ascorbic acid (AA). Bamboolike CNTs, commercial CNTs (diameter ca. 20 nm; see Figure S7), and commercial Pt/C (10 wt %) were used as reference catalysts for comparison.

Cyclic voltammograms (CVs) were first recorded in oxygen-saturated 0.1 M KOH electrolyte (see Figure S8). The N-graphene/CNT hybrid showed a net peak current density of 0.99 mA cm^{-2}, which was three times higher than that of commercial Pt/C catalysts (0.28 mA cm^{-2}). The N-graphene/CNT hybrid also showed significantly improved performance as compared with that of commercial CNTs and a bulk Pt electrode, which either showed a remarkable negative shift of the onset potential or a prominent decrease in the net peak current density (see Figure S9). We recorded rotating disk electrode (RDE) voltammograms to study the electrochemical catalytic activity for ORR (Figure 3a). Although the onset potential at the N-graphene/CNT electrode (−0.08 V) was slightly more negative than that at the Pt/C electrode (−0.03 V), N-graphene/CNT presented an enhanced limited current density as compared with Pt/C. These results indicate that the N-graphene/CNT hybrid possesses comparable catalytic activity to that of the commercial Pt/C catalyst. Koutecky–Levich plots (Figure 3b) for the N-graphene/CNT hybrid at different rotation rates exhibited good parallel linearity between the inverse current density (J^{-1}) and the inverse of the square root of the rotation rate ($\omega^{-1/2}$) at different potential values, thus suggesting first-order kinetics of ORR on the N-graphene/CNTs. The electron-transfer number and kinetic current density for ORR on the N-graphene/CNTs were calculated as 3.98 and 5.6 mA cm^{-2} at −0.25 V, thus indicating that ORR proceeded through a four-electron-transfer route with water production at the N-graphene/CNT electrode; this result was reconfirmed by tests with a rotating ring–disk electrode (RRDE; see Figure S10a). Notably, the N-graphene/CNT hybrid also showed excellent stability (see Figure S10b).

The N-graphene/CNT hybrid also showed excellent catalytic activity for the water-oxidation reaction, as assessed with a RDE system. Figure 3c shows the results of linear sweep voltammetry (LSV) on various electrodes at an RDE rotation speed of 1500 rpm. The peak at around 1.4 V for the N-graphene/CNT hybrid could be attributed to the redox process of Fe nanocatalysts or induced by nitrogen doping. The N-graphene/CNT hybrid attained a current density of 10 mA cm^{-2} at a potential of 1.65 V, which is almost 0.2 V lower than that of the Pt/C catalyst (1.83 V). The overpotential for yielding a current density of 10 mA cm^{-2} on the N-graphene/CNTs was also comparable to that found for previously reported catalysts.[13g,16] We also recorded RRDE voltammograms to monitor the intermediate products during the water oxidation. In this way, we could infer whether the water oxidation on N-graphene/CNT catalysts proceeded through a four-electron route to form O_2 or a two-electron pathway to form H_2O_2.[17] Therefore, a given potential was applied to the platinum ring electrode in two separate RRDE tests to monitor whether any O_2 or H_2O_2 was produced at the disk electrode. Specifically, the ring potential was set as 0.6 V for the detection of O_2 reduction and 1.5 V for the measurement of H_2O_2 oxidation. At a scan potential ranging from 1.0 to 1.9 V, almost no oxidation current was observed at the ring electrode setting of 1.5 V (Figure 3d), thus suggesting that a negligible amount of H_2O_2 formed in this process. In contrast, when the ring electrode was set to 0.6 V, an apparent

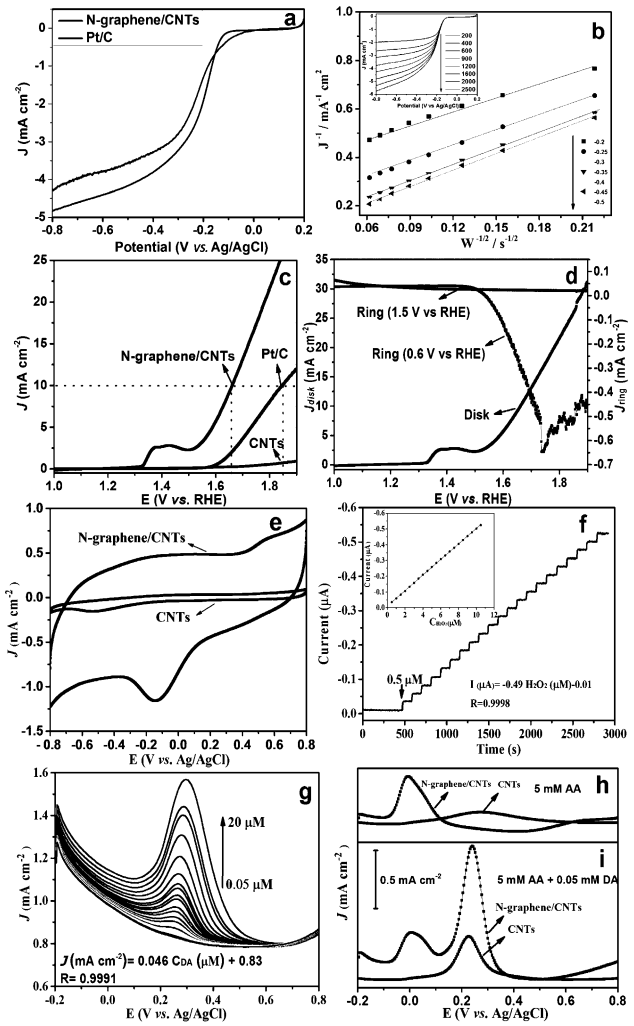

Figure 3. a) LSV curves of the N-graphene/CNT (black) and Pt/C electrode (gray) at a rotation rate of 1600 rpm. b) Koutecky–Levich plot of current density versus $\omega^{-1/2}$ at different potentials on the N-graphene/CNT electrode; the inset shows polarization curves of ORR. c) Water-oxidation activity of the N-graphene/CNT, Pt/C (10%), and commercial CNT electrode in Ar-saturated 0.1 M KOH; rotation speed: 1500 rpm, scan rate: 5 mV s^{-1}. d) RRDE measurement of ring current density recorded at the platinum ring electrode maintained at 1.5 or 0.6 V (vs. RHE) in Ar-saturated 0.1 M KOH solution and the related current density at the N-graphene/CNT disk electrode; rotation speed: 1500 rpm, scan rate: 5 mV s^{-1}. e) CVs of N-graphene/CNT hybrids and CNTs in 0.1 M phosphate buffer solution (phosphate-buffered saline, pH 7.4) containing 0.1 mM H_2O_2. f) Amperometric response of the N-graphene/CNT hybrid upon the repeated addition of 0.5 M H_2O_2 at regular intervals at an applied potential of −0.1 V; the inset shows the linear relationship between the response current and the H_2O_2 concentration. g) DPV curves for different concentrations of DA at the N-graphene/CNT electrode in PBS solution (pH 7.4). h) DPV curves of CNTs and N-graphene/CNTs in 0.1 M PBS solution containing 5 mM AA. i) DPV curves of CNTs and N-graphene/CNTs in 0.1 M PBS solution containing 5 mM AA and 0.05 mM DA.

reduction current starting at around 1.5 V was observed owing to the evolution of oxygen. These results demonstrate that the N-graphene/CNT hybrid catalyzes water oxidation through a four-electron route with the production of O_2. Notably, the N-graphene/CNT hybrid also showed excellent durability for water oxidation in alkaline solutions. The N-graphene/CNT hybrid even showed a slight increase in current density when continuously operating at a constant potential of 1.65 V for 2 h (see Figure S11). In contrast, the Pt/C catalysts showed a clear decrease in current density under the same conditions.

We further studied the electrochemical response to H_2O_2 on the N-graphene/CNT-modified GCE. Figure 3e shows CVs for N-graphene/CNT and CNT electrodes in the presence of 0.1 mM H_2O_2. The N-graphene/CNT hybrid showed significantly improved activity as compared with CNTs. To be specific, the N-graphene/CNT hybrid exhibited a reduction peak at −0.1 V corresponding to the reduction of H_2O_2; this value was much higher than that found for the CNTs (−0.53 V). Furthermore, the N-graphene/CNT hybrid displayed a net peak current density of 0.68 mA cm^{-2}, which is four times higher than that of the CNTs (0.15 mA cm^{-2}). The N-graphene/CNT electrode responded rapidly, within 3 s, to the addition of H_2O_2 and showed a good linear relationship between the current signal and the H_2O_2 concentration in the range of 0.5–10.5 μM, with a correlation coefficient of 0.9998 (Figure 3f). More importantly, an ultralow detection limit of around 8.6 nM based on $S/N = 3$ was observed for the N-graphene/CNT electrode, as well as an ultrahigh sensitivity of about 6.93 A M^{-1} cm^{-2}. The N-graphene/CNT electrode is thus one of the most competitive enzyme-free H_2O_2 sensors in terms of detection limit and sensitivity (see Table S1 in the Supporting Information).[18] Such N-graphene/CNT hybrids therefore have great potential for the fabrication of various oxidase-based biosensors. We investigated a glucose biosensor as an example by loading glucose oxidase enzyme (GOD) on the N-graphene/CNT electrode. The resulting electrode N-graphene/CNT–GOD–GCE showed good performance in the detection of glucose, including a rapid response, excellent stability, good repeatability, and high sensitivity (see Figure S12).

We further investigated the electrochemical catalytic properties of the N-graphene/CNT hybrid by studying its electrochemical response to dopamine (DA; see Figure S13), an important neurotransmitter that affects the brain processes that control movement, emotional response, and the capacity to feel pleasure and pain. The N-graphene/CNT electrode showed a highly sensitive response to DA, as based on differential pulse voltammetry (DPV; Figure 3g), with a good linear relationship ranging from 0.05 to 20 μM and a correlation coefficient of 0.993 (see Figure S13c). Furthermore, the N-graphene/CNT electrode had a detection sensitivity as high as 4.6 A M^{-1} cm^{-2} and a lower detection limit of 9.7 nM at $S/N = 3$. These performance parameters demonstrate that the DA sensor based on the N-graphene/CNT hybrid possesses advantages over previously reported electrochemical sensors (see Table S2).[19] Figure 3h,i show the DPV response to AA and DA at CNT and N-graphene/CNT electrodes. The N-graphene/CNT hybrid also manifested remarkably improved catalytic activity for the oxidation of DA and AA as compared with CNTs. Upon the addition of 5 mM AA, the N-graphene/CNT electrode showed a peak current three times higher and a remarkable negative shift (more than 0.25 V) of the peak potential relative to those of the commercial CNT electrode. Furthermore, the N-graphene/

CNT electrode displayed two separated oxidation peaks corresponding to the oxidation of AA and DA in an electrolyte consisting of 5 mM AA and 0.05 mM DA. However, the CNTs showed overlapping peaks and a much weaker peak current density. These results indicate that the N-graphene/CNT hybrid also shows excellent catalytic activity for the oxidation of AA and DA and provides an effective electrochemical sensing platform for the simultaneous determination of AA and DA.

The N-graphene/CNT hybrids also showed an enhanced current density and a decreased overpotential in comparison with bamboolike CNTs for the electrochemical reactions of ORR, water oxidation, H_2O_2 reduction, and redox reactions of DA (see Figure S14). The outstanding electrocatalytic activity can be attributed to the unique morphology and defect structures of the N-graphene/CNT hybrids. On one hand, the N-graphene/CNTs have an open-end structure with a diameter around 100 nm, which makes it possible for ions/electrolyte to infiltrate and be transported into the inner void of the CNT. As a result, the small graphene nanosheets inside the CNTs, which have a large number of active sites owing to edge effects, can get access to the electroactive molecules, thus leading to remarkably enhanced activity. On the other hand, the N-graphene/CNTs have a considerable N-doping concentration and contain iron-based nanocatalysts, both of which can contribute to the improvement of catalytic activity for the corresponding reactions.[12,20]

In summary, we have successfully developed a facile method for the one-pot, one-step synthesis from solid-phase sources of a carbon nanoarchitecture with graphene nanosheets grown in CNT voids. The facile procedure for the synthesis of the N-graphene/CNTs, together with their excellent catalytic activity, may open up a promising avenue for the development of multifunctional electrocatalysts for a variety of applications.

Received: February 19, 2014
Published online: May 5, 2014

Keywords: carbon nanotubes · electrocatalysts · graphene · hybrid materials · nitrogen doping

[1] a) S. Stankovich, D. A. Dikin, G. H. B. Dommett, K. M. Kohlhaas, E. J. Zimney, E. A. Stach, R. D. Piner, S. T. Nguyen, R. S. Ruoff, *Nature* **2006**, *442*, 282; b) R. H. Baughman, A. A. Zakhidov, W. A. de Heer, *Science* **2002**, *297*, 787.

[2] a) T.-K. Hong, D. W. Lee, H. J. Choi, H. S. Shin, B.-S. Kim, *ACS Nano* **2010**, *4*, 3861; b) K. H. Kim, Y. Oh, M. F. Islam, *Nat. Nanotechnol.* **2012**, *7*, 562; c) J. Pyun, *Angew. Chem.* **2011**, *123*, 46; *Angew. Chem. Int. Ed.* **2011**, *50*, 46; d) D. Yu, L. Dai, *J. Phys. Chem. Lett.* **2010**, *1*, 467.

[3] a) M.-Q. Zhao, X.-F. Liu, Q. Zhang, G.-L. Tian, J.-Q. Huang, W. Zhu, F. Wei, *ACS Nano* **2012**, *6*, 10759; b) V. C. Tung, L.-M. Chen, M. J. Allen, J. K. Wassei, K. Nelson, R. B. Kaner, Y. Yang, *Nano Lett.* **2009**, *9*, 1949.

[4] a) V. Sridhar, H.-J. Kim, J.-H. Jung, C. Lee, S. Park, I.-K. Oh, *ACS Nano* **2012**, *6*, 10562; b) S. S. Jyothirmayee Aravind, R. I. Jafri, N. Rajalakshmi, S. Ramaprabhu, *J. Mater. Chem.* **2011**, *21*, 18199; c) B. P. Vinayan, R. Nagar, V. Raman, N. Rajalakshmi, K. S. Dhathathreyan, S. Ramaprabhu, *J. Mater. Chem.* **2012**, *22*, 9949; d) Z. Fan, J. Yan, L. Zhi, Q. Zhang, T. Wei, J. Feng, M. Zhang, W. Qian, F. Wei, *Adv. Mater.* **2010**, *22*, 3723.

[5] Y. Zhu, L. Li, C. Zhang, G. Casillas, Z. Sun, Z. Yan, G. Ruan, Z. Peng, A.-R. O. Raji, C. Kittrell, R. H. Hauge, J. M. Tour, *Nat. Commun.* **2012**, *3*, 1225.

[6] Y. Li, W. Zhou, H. Wang, L. Xie, Y. Liang, F. Wei, J.-C. Idrobo, S. J. Pennycook, H. Dai, *Nat. Nanotechnol.* **2012**, *7*, 394.

[7] R. Lv, T. Cui, M.-S. Jun, Q. Zhang, A. Cao, D. S. Su, Z. Zhang, S.-H. Yoon, J. Miyawaki, I. Mochida, F. Kang, *Adv. Funct. Mater.* **2011**, *21*, 999.

[8] a) Z. Sun, Z. Yan, J. Yao, E. Beitler, Y. Zhu, J. M. Tour, *Nature* **2010**, *468*, 549; b) Y. Shen, L. Yan, H. Song, J. Yang, G. Yang, X. Chen, J. Zhou, Z.-Z. Yu, S. Yang, *Angew. Chem.* **2012**, *124*, 12368; *Angew. Chem. Int. Ed.* **2012**, *51*, 12202.

[9] a) Y. Tang, B. L. Allen, D. R. Kauffman, A. Star, *J. Am. Chem. Soc.* **2009**, *131*, 13200; b) X. Qi, Y. Deng, W. Zhong, Y. Yang, C. Qin, C. Au, Y. Du, *J. Phys. Chem. C* **2010**, *114*, 808; c) Y. Chai, Q. F. Zhang, J. L. Wu, *Carbon* **2006**, *44*, 687; d) M. Lin, J. P. Y. Tan, C. Boothroyd, K. P. Loh, E. S. Tok, Y.-L. Foo, *Nano Lett.* **2007**, *7*, 2234.

[10] Z. Wen, S. Ci, F. Zhang, X. Feng, S. Cui, S. Mao, S. Luo, Z. He, J. Chen, *Adv. Mater.* **2012**, *24*, 1399.

[11] a) A. Fischer, J. O. Mueller, M. Antonietti, A. Thomas, *ACS Nano* **2008**, *2*, 2489; b) Y.-S. Jun, W. H. Hong, M. Antonietti, A. Thomas, *Adv. Mater.* **2009**, *21*, 4270.

[12] a) R. T. K. Baker, M. A. Barber, P. S. Harris, F. S. Feates, R. J. Waite, *J. Catal.* **1972**, *26*, 51; b) G. D. Nessim, *Nanoscale* **2010**, *2*, 1306.

[13] a) J. C. Carrero-Sánchez, A. L. Elías, R. Mancilla, G. Arrellín, H. Terrones, J. P. Laclette, M. Terrones, *Nano Lett.* **2006**, *6*, 1609; b) K. Gong, F. Du, Z. Xia, M. Durstock, L. Dai, *Science* **2009**, *323*, 760; c) L. Qu, Y. Liu, J.-B. Baek, L. Dai, *ACS Nano* **2010**, *4*, 1321; d) S. Ci, Z. Wen, J. Chen, Z. He, *Electrochem. Commun.* **2012**, *14*, 71; e) Z. Wen, X. Wang, S. Mao, Z. Bo, H. Kim, S. Cui, G. Lu, X. Feng, J. Chen, *Adv. Mater.* **2012**, *24*, 5610; f) W. Li, Z. Zhang, B. Kong, S. Feng, J. Wang, L. Wang, J. Yang, F. Zhang, P. Wu, D. Zhao, *Angew. Chem.* **2013**, *125*, 8309; *Angew. Chem. Int. Ed.* **2013**, *52*, 8151; g) Y. Zhao, R. Nakamura, K. Kamiya, S. Nakanishi, K. Hashimoto, *Nat. Commun.* **2013**, *4*, 1.

[14] a) S. van Dommele, A. Romero-Izquirdo, R. Brydson, K. P. de Jong, J. H. Bitter, *Carbon* **2008**, *46*, 138; b) D. Wei, Y. Liu, Y. Wang, H. Zhang, L. Huang, G. Yu, *Nano Lett.* **2009**, *9*, 1752.

[15] A. A. Koós, F. Dillon, E. A. Obraztsova, A. Crossley, N. Grobert, *Carbon* **2010**, *48*, 3033.

[16] a) E. Ortel, T. Reier, P. Strasser, R. Kraehnert, *Chem. Mater.* **2011**, *23*, 3201; b) Y. Y. Liang, Y. G. Li, H. L. Wang, J. G. Zhou, J. Wang, T. Regier, H. J. Dai, *Nat. Mater.* **2011**, *10*, 780; c) M. R. Gao, Y. F. Xu, J. Jiang, Y. R. Zheng, S. H. Yu, *J. Am. Chem. Soc.* **2012**, *134*, 2930.

[17] a) E. Mirzakulova, R. Khatmullin, J. Walpita, T. Corrigan, N. M. Vargas-Barbosa, S. Vyas, S. Oottikkal, S. F. Manzer, C. M. Hadad, K. D. Glusac, *Nat. Chem.* **2012**, *4*, 794; b) W. Rüttinger, G. Dismukes, *Chem. Rev.* **1997**, *97*, 1.

[18] a) W. Chen, S. Cai, Q.-Q. Ren, W. Wen, Y.-D. Zhao, *Analyst* **2012**, *137*, 49; b) S. Chen, R. Yuan, Y. Chai, F. Hu, *Microchim. Acta* **2013**, *180*, 15.

[19] K. Jackowska, P. Krysinski, *Anal. Bioanal. Chem.* **2013**, *405*, 3753.

[20] a) A. Ambrosi, S. Y. Chee, B. Khezri, R. D. Webster, Z. Sofer, M. Pumera, *Angew. Chem.* **2012**, *124*, 515; *Angew. Chem. Int. Ed.* **2012**, *51*, 500; b) A. Ambrosi, C. K. Chua, B. Khezri, Z. Sofer, R. D. Webster, M. Pumera, *Proc. Natl. Acad. Sci. USA* **2012**, *109*, 12899; c) C. E. Banks, A. Crossley, C. Salter, S. J. Wilkins, R. G. Compton, *Angew. Chem.* **2006**, *118*, 2595; *Angew. Chem. Int. Ed.* **2006**, *45*, 2533; d) C. H. A. Wong, C. K. Chua, B. Khezri, R. D. Webster, M. Pumera, *Angew. Chem.* **2013**, *125*, 8847; *Angew. Chem. Int. Ed.* **2013**, *52*, 8685.

